Available online at www.sciencedirect.com
ScienceDirect
Energy Conversion and Management 49 (2008) 1182–1192
ENERGY CONVERSION & MANAGEMENT
www.elsevier.com/locate/enconman

Predicting distributions of wear sites on shell wall of feedwater heater in nuclear power plant using two phase models

Y.M. Ferng [a,*], C.T. Hung [b]

[a] Nuclear Science and Technology Development Center, 101, Sec. 2, Kuang-Fu Road, Hsinchu 30013, Taiwan, ROC
[b] Maintenance Department, Maanshan Nuclear Power Plant, Taiwan Power Company, Taiwan, ROC

Received 19 January 2007; accepted 9 September 2007
Available online 23 October 2007

Abstract

Severe wall thinning may cause a leak on the feedwater heaters (FWHs) shell wall, which could result in the nuclear power plant derating or shutdown, even personal fatalities. This wall thinning of FWHs shell is essentially engendered by droplet impingement wear, which is strongly related to the two phase flow characteristics within the shell side. In this paper, two phase models are proposed to investigate the characteristics of droplet flow and predict the distributions of impingement wear sites for the FWHs. These models include the Eulerian/Lagrangian droplet type two phase models and the droplet impingement wear model. Based on the simulation results, the flow models can reasonably capture the three dimensional distribution of droplet flow and its rebound characteristics within the FWHs shell side. Coupled with these flow characteristics, an appropriate indicator, derived from the droplet impingement wear model, is used to predict the severe wear sites on the FWHs shell wall. The predicted wear sites agree well with the plant measured data for the selected nuclear power plant. The unsymmetrical distribution patterns of wear sites are also precisely captured. These correspondences show that the two phase models presented herein can be used to investigate the flow characteristics and impingement wear for FWHs in the nuclear power plant.

Keywords: Wear sites; Feedwater heater; Two phase models

1. Introduction

A feedwater heater (FWH) is essential equipment to improve the efficiency for a nuclear power plant. In this process, steam is extracted from different stages of the turbines and delivered to the shell side of a FWH. Condensate is pumped to its tube side. The shell side steam heat is then transferred to the condensate, resulting in an improvement of plant efficiency by increasing the boiler inlet temperature. The possible impacts for failure of FWHs include reduction of the thermal efficiency due to inadequate heating of the feedwater, overloading the turbine and other FWHs, plant derating or shutdown and even staff injury. On January 18, 1999, a thru-wall leak was found on the #3 low pressure FWH shell wall at Susquehanna Unit #2. This leak size was about $1/2'' \times 1 - 1/2''$. In the same year, two rectangular holes of about $1/2'' \times 1 - 1/2''$ each were found on a #3 low pressure FWH shell wall at the Boston Edison Pilgrim Station. On May 14, 1999, a fish-mouth leak occurred on the shell side of #4 low pressure FWH at the Point Beach Unit 1. This leak size is about $27''$ long and $7/8''$ wide. All these leaks of FWHs shell walls were believed to result from droplet impingement wear, which resulted in the power plant derating or shutdown and even caused the staff injury event. Therefore, the plant staff has paid much attention on the shell failure for FWHs since then.

These impingement wear phenomena on the FWH shell wall are strongly associated with the flow characteristics within the shell side. Therefore, flow models are proposed in this paper to investigate the flow behaviors within the FWH shell side and predict the impingement wear sites on the shell wall. Since the flow characteristics within the

* Corresponding author. Fax: +886 3 5715131x4202.
E-mail address: ymferng@ess.nthu.edu.tw (Y.M. Ferng).

0196-8904/$ - see front matter © 2007 Elsevier Ltd. All rights reserved.
doi:10.1016/j.enconman.2007.09.012

FWH shell side essentially belong to the droplet type two phase flow system, the flow models presented herein include the droplet type two phase model and the droplet impingement wear model. The droplet flow within the shell side can be considered as a dispersed flow that is characterized by the coexistence of continuous flow (vapor flow) and particle flow (droplet flow). This dispersed two phase flow can be reasonably simulated using the Eulerian/Lagrangian model [1–14] that treats the continuous phase through an Eulerian approach and the dispersed phase through a Lagrangian approach, respectively. In addition, there are more than a hundred tubes in the heat exchanger bundles in the FWH shell side, which are arranged so tightly that they can be reasonably treated as a porous medium [15,16].

The simulated FWHs are those in a pressurized water reactor (PWR) that is located in the southern tip of Taiwan. According to the simulation results, the three dimensional characteristics of droplet flow in the FWH shell side can be reasonably simulated by the Eulerian/Lagrangian two phase model, which includes the droplet flow paths, droplet impingement and droplet rebound behaviors on the solid wall. Coupled with these droplet flow characteristics, an appropriate indicator, derived from the droplet impingement wear model, is used to predict the severe wear sites on the shell wall, which is essentially similar to previous works [17–19]. The predicted wear sites for different FWHs are compared with plant data measured by the staff during the plant outage, which demonstrates the good agreement. These results reveal that the two phase models proposed in this paper can be used to investigate reasonably the flow characteristics, droplet impingement and associated wear for the FWHs of the nuclear power plant.

2. Two phase models

Fig. 1 schematically shows a horizontal, closed, two zone FWH. This two zone FWH typically consists of a condensing zone and a drain cooling zone. A condensing zone is the major internal section for a FWH [20], which contains a large amount of tube surface area to condense all of the incoming steam. The drain cooling zone is used to preheat the feedwater before it enters the condensing zone of the next heater. An impingement plate is placed on the opposite side of the inlet tube, which is used to protect the tube bundle from droplets impingement. As mentioned in the previous section, the Eulerian/Lagrangian flow approaches are adopted herein since the flow characteristic with the FWH shell side is the droplet type two phase flow system. All the equations for the two phase models are described in the following subsections.

2.1. Eulerian/Lagrangian flow models

Several appropriate assumptions are needed to derive this Eulerian/Lagrangian flow model and are presented as follows:

1. The droplet flow in the FWH shell side can be considered as a dilute two phase flow. Interactions between droplets can be neglected.
2. Droplets in the two phase flow can be considered as ideal spheres with a constant size of 1 mm.
3. The swirling effect of droplets is not considered in the models.
4. The drag force between the two phases is only considered in the momentum equation of the droplet.
5. Perfect rebound characteristics are assumed in the droplet-wall collision process.
6. Turbulence induced by the existence of droplets in the steam flow is only considered in the dispersion of droplets.

2.1.1. Eulerian approach for the continuous phase

The Eulerian mathematical model simulating the flow characteristics for the continuous phase (i.e. steam flow) consists of the continuity equation, momentum equation and turbulent models. These equations are essentially derived from the conservation laws, which are so-called first principle equations.

Continuity equation

$$\nabla \cdot (\rho \vec{U}) = 0 \tag{2.1}$$

where $\rho =$ steam density and $\vec{U} =$ steam velocity vector

Momentum equation

$$\nabla \cdot (\rho \vec{U} \vec{U}) = -\nabla P + \nabla \cdot (\mu * \nabla \vec{U}) - \nabla P_{\text{porus}} \tag{2.2}$$

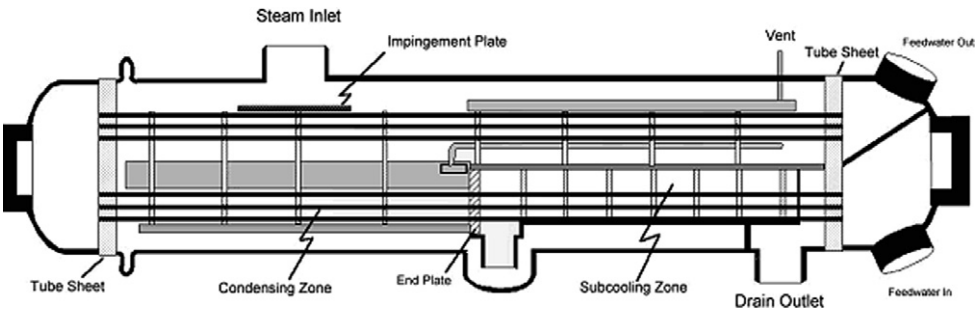

Fig. 1. Schematic of a typical two zone FWH.

where

$$\mu* = \mu_\ell + \mu_t, \tag{2.3}$$

in which μ_ℓ = steam viscosity, μ_t = turbulence induced viscosity estimated by the turbulent model that will be presented in the following subsection, P = steam pressure and $-\nabla P_{porous}$ = extra pressure drop due to the existence of tube bundles in the steam flow, which consists of Darcy drag and Forchheimer drag. This Darcy–Forchheimer drag force has the following form [21,22].

$$-\nabla P_{porous} = \frac{\mu_\ell \vec{U}}{\kappa} + \frac{F\bar{\rho}|U|\vec{U}}{\sqrt{\kappa}} \tag{2.4}$$

The permeability κ and inertial coefficient F are defined as [23]

$$\kappa = \frac{\varepsilon^3 d^2}{150(1-\varepsilon)^2} \tag{2.5}$$

$$F = \frac{1.75}{\sqrt{150}\varepsilon^{1.5}} \tag{2.6}$$

In which ε = porosity of tube bundles and d = tube diameter

Turbulent models The turbulence induced shear stress and heat flux can be expressed by the Boussinseq concept. Then,

$$-\overline{\rho u' v'} = \mu_t \frac{\partial u}{\partial n} \tag{2.7}$$

and

$$\mu_t = C_\mu \bar{\rho} k^2/\varepsilon, \tag{2.8}$$

where superscript ‘means the fluctuation term for the flow parameter and u = velocity along the wall, n = distance normal to the wall, k = turbulent kinetic energy and ε = turbulent energy dissipation rate.

k and ε can be obtained by the transport equations of these turbulent quantities, which are expressed as follows:

$$\nabla\cdot(\rho\vec{U}k) = \nabla\cdot\left[\left(\mu_\ell + \frac{\mu_t}{\sigma_k}\right)\nabla k\right] + G_k - \rho\varepsilon \tag{2.9}$$

$$\nabla\cdot(\rho\vec{U}\varepsilon) = \nabla\cdot\left[\left(\mu_\ell + \frac{\mu_t}{\sigma_\varepsilon}\right)\nabla\varepsilon\right] + \frac{\varepsilon}{k}(C_{\varepsilon1}G_k - C_{\varepsilon2}\rho\varepsilon) \tag{2.10}$$

where

$$G_k = \text{turbulence generation term} = \mu^*\nabla\vec{U}\cdot\left[\nabla\vec{U} + (\nabla\vec{U})^T\right] \tag{2.11}$$

C_μ, $C_{\varepsilon1}$, $C_{\varepsilon2}$, σ_k, σ_ε are empirical constants for the turbulent models and are illustrated in Table 1 [24].

2.1.2. Lagrangian approach for the disperse phase

In order to capture the rebound characteristics of the droplets within the FWH shell side, the Lagrangian approach is used in the simulation work. The Lagrangian equations [13,14,25] for each droplet can be described as follows:

Position equation

$$\frac{dx_p}{dt} = \vec{U}_p \tag{2.12}$$

where x_p = position of droplet, $\vec{U}_p$ = velocity vector of droplet.

Momentum equation

$$m_p\frac{d\vec{U}_p}{dt} = \vec{F} \tag{2.13}$$

where m_p = mass of droplet,

$$\vec{F} = \text{total force vectors acting on the droplet} = \vec{F}_D + \vec{F}_P + \vec{F}_B, \tag{2.14}$$

$$\vec{F}_D = \text{drag force} = \frac{1}{8}\pi D^2\rho C_D|\vec{U}_R|\vec{U}_R \tag{2.15}$$

$$\vec{F}_P = \text{pressure gradient force} = -\frac{1}{4}\pi D^3\nabla P \tag{2.16}$$

$$\vec{F}_B = \text{buoyancy force} = \frac{1}{6}\pi D^3(\rho_P - \rho)\vec{g} \tag{2.17}$$

D = droplet diameter and ρ_P = droplet density

$$C_D = \text{drag factor} = \max\left\{0.44, \frac{24}{Re_P}\left(1 + 0.15Re_P^{0.687}\right)\right\}\text{[26]} \tag{2.18}$$

$$Re_p = \text{droplet Reynolds number} = \frac{\rho|\vec{U}_R|D}{\mu} \tag{2.19}$$

$$\vec{U}_R = \text{relative velocity vector between the steam and droplet phases} = \vec{U} - \vec{U}_p \tag{2.20}$$

2.2. Droplet impingement wear model

The two phase system in the FWH shell is a high quality droplet type wet system. In this system, the droplets are carried by the high velocity steam. Some of them may impinge on the oxide layer of the metal with high kinetic energy, erode the oxide layer from the shell wall and subsequently cause wall thinning, which is the so called droplet impingement wear. Many parameters affect the sophisticated droplet impingement wear. A model simply describes this phenomenon as one where the oxide layer is removed by the action of numerous individual impacts of liquid droplets [27]. Its formula can be expressed as

$$\dot{m} = C_s N F(\theta)\frac{\rho_p u_n^2}{HV} \tag{2.21}$$

Table 1
Constants of turbulent models

C_μ	$C_{\varepsilon1}$	$C_{\varepsilon2}$	σ_k	σ_ε	σ_t
0.09	1.44	1.92	1.0	1.3	0.9

where $\dot{m}$ = wear rate, C_s = system constant, N = frequency, $F(\theta)$ = characteristic function,

θ = impact angle, HV = wall hardness, u_n = normal velocity of droplet = $(\vec{U}_p \cdot \vec{n})$ (2.22)

and $\vec{n}$ = normal vector of wall.

The above equation demonstrates that the metal loss by droplet impingement wear is proportional to the density of the liquid droplets and the square of their normal velocities. In other words, the wear severity is strongly related to the kinetic energies of the droplets. Therefore, $\rho_P u_n^2$ is an appropriate indicator to predict reasonably the severe wear sites on the wall surface, which is similar to previous works [17–19].

2.3. Boundary conditions

The two phase models to simulate the three dimensional characteristics of droplet flow and impingement wear sites within the FWH have been described in the previous sections. Appropriate boundary conditions are needed to solve the whole problem. The inlet boundary conditions for all the calculations are specified based on the design conditions of the FWHs. The outlet pressure is needed for the outlet boundary condition and is set to the design pressure of the drain cooling zone. Since the behaviors of the turbulent steam flow change abruptly near the wall, the wall function method [28] is adopted in the hydraulic simulation for the velocity and turbulent distributions to avoid the need for finer grids near the wall. In addition, the restitution coefficient [13,14,25,29–34] is used to simulate the rebound behavior as liquid droplets collide with the impingement plate and shell wall.

3. Numerical treatment

3.1. Grid model

Fig. 2 typically demonstrates the schematic of grid models for the FWH simulated in this paper, which is a low pressure one of the pressurized water reactor (PWR) located in the south tip of Taiwan. Fig. 2a is a whole picture of this grid model in a three dimensional presentation. The space coordinate is shown in the left portion and the direction of this FWH layout is indicated at the upper right corner. Fig. 2b shows the grid distributions inside the FWH shell side. The yellow portion represents the grids projected on the tube support plates; the red portion represents the grids projected on the impingement plate; the purple and gray regions represent the grids on the drain cooling zone and inlet elbow, respectively. Fig. 2c shows the two dimensional grid distributions from the front view. A non-uniform grid distribution is adopted in this simulation. More grids are needed around the impingement plate and shell wall in order to capture precisely the rebound characteristics of the liquid droplets. There are 420 meshes on the axial cross section and 160 grids along the axial direction within this FWH shell side.

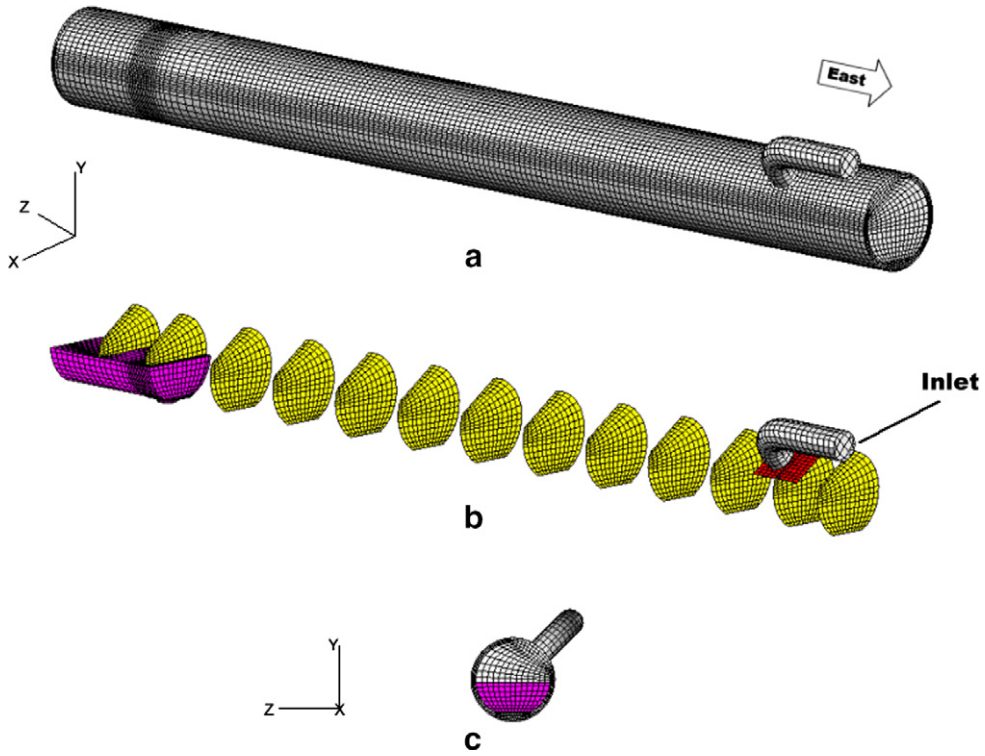

Fig. 2. Schematics of gird models for a FWH.

3.2. Numerical scheme

Coupled with appropriate boundary conditions, a set of equations describing the hydraulic phenomena of droplet type two phase flow within the FWH has been presented in the previous section. These governing equations essentially are non-linear partial differential equations. Using the control volume approach, these differential form equations are discretized into finite difference forms for numerical calculations. The details of the control volume approach for the finite difference method can be referred to the work of Patankar [35]. A hybrid scheme is used to treat the convection terms coupled with the diffusion terms in the transport equations for velocity and turbulent parameters. The finite differencing forms of the velocity equations are coupled with pressure, which can be solved by the so-called SIMPLE scheme [36]. In addition, the geometry in the FWH shell side is not of simple rectangular or cylindrical system. A body fitted coordinate (BFC) [37] method is adopted to deal with this complicated multi-dimensional geometry. The numerical procedures to solve the Eulerian/Lagrangian flow model and droplet impingement wear model are described as follows:

1. Set the boundary conditions based on the plant designed values, including the distributions of inlet steam flow and droplet velocities, outlet pressure.
2. Solve the momentum Eq. (2.2) to determine the steam flow field in the FWH.
3. Solve the pressure correction equation [35] derived from the continuity Eq. (2.1) to eliminate the mass conservation error and then apply appropriate corrections [35] to the steam velocity and pressure fields.
4. Solve the two equation model (2.9) and (2.10) for the turbulent properties and update the steam flow effective properties that are induced by the flow turbulence.
5. Solve the droplet position and momentum Eqs. ((2.12)–(2.20)) to determine the position and velocity of each liquid droplet within the FWH shell side.
6. Repeat steps 2–6 until the convergence criteria are satisfied.
7. After obtaining the converged results of the droplets characteristics, the appropriate indicator $\rho_P u_P^2$ can be used to predict the severe wear sites on the FWH shell wall.

The convergence criteria in the simulation are set as that summation of the relative residual in every control volumes for each governing equations is smaller than 10^{-3}. The CFD code-CFX4 (computational fluid dynamics) [25] is used in this paper. All of the calculations are performed on the Pentium IV 3.0 G PC.

4. Results and discussion

As aforementioned descriptions, the leaks of the FWH shell wall are believed to result from droplet impingement. This wear is essentially caused by the droplets carried by the incoming steam colliding with the impingement plate, rebounding dispersedly and impinging on the shell wall as schematically shown in Fig. 3. These phenomena can be reasonably captured by the present Eulerian/Lagrangian two phase models, which is clearly shown in Fig. 4. The simulated FWH in Fig. 4 is a high pressure one that is connected with the high pressure turbine (HPTB) through extraction system piping. The flow conditions of

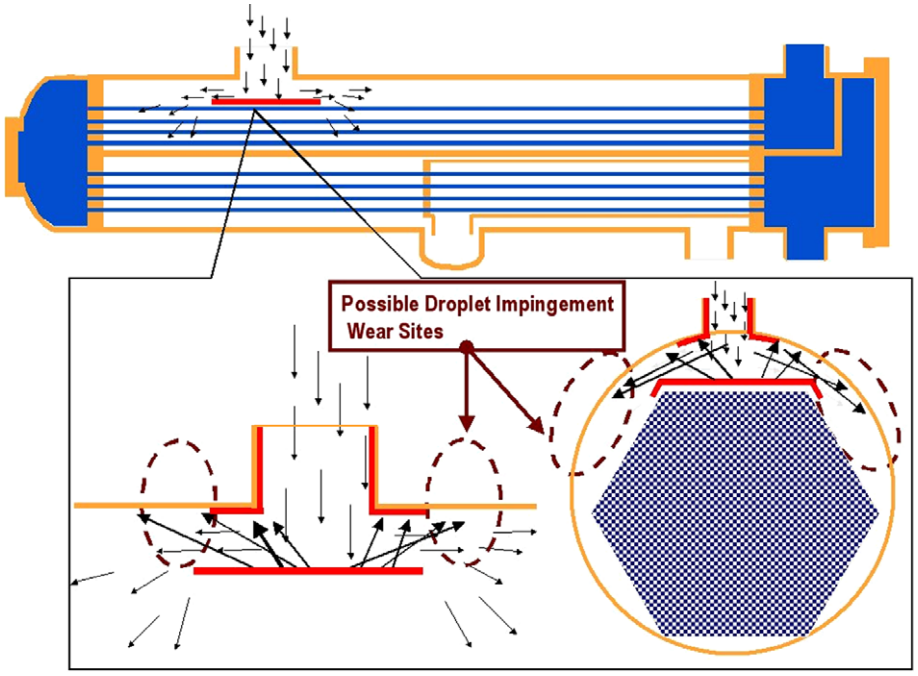

Fig. 3. Schematic of droplet impingement within a FWH.

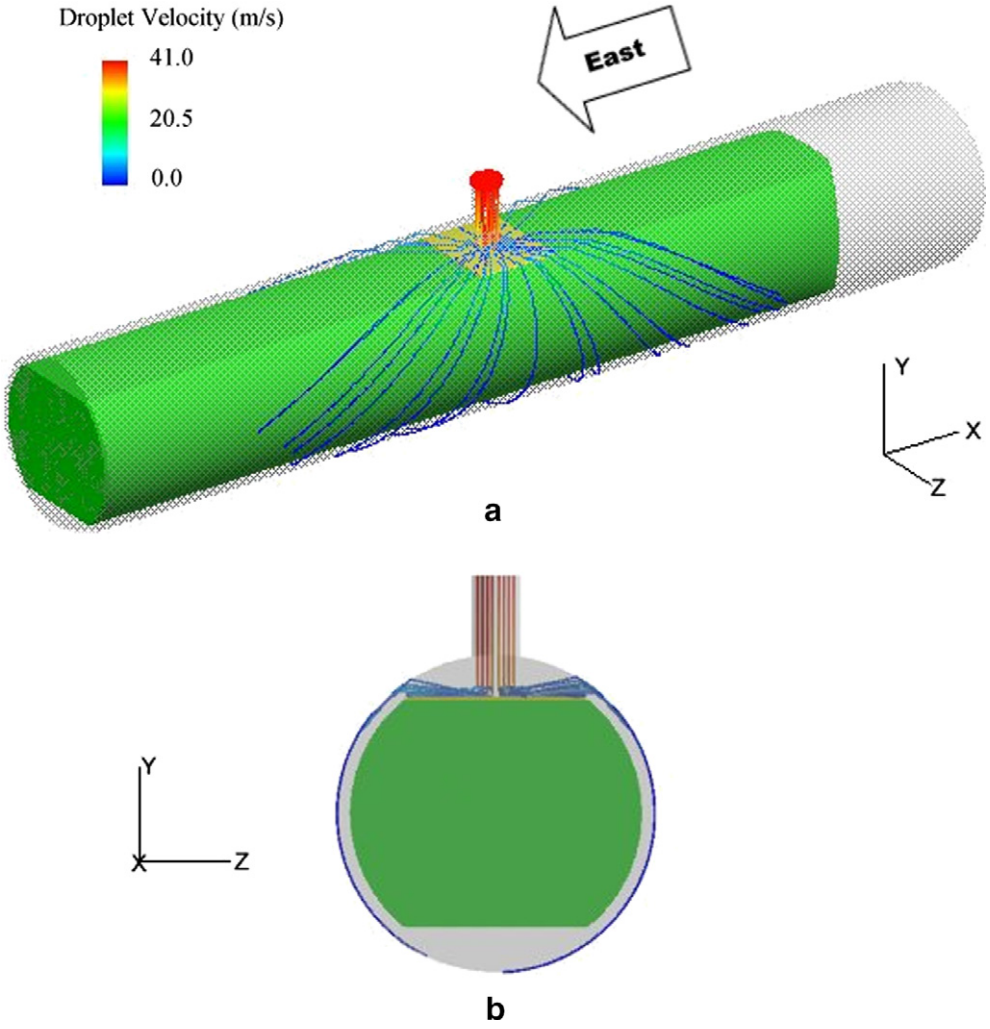

Fig. 4. Flow characteristics of liquid droplets within a high pressure FWH shell.

the inlet steam for this FWH are that the inlet temperature is 451 °F, inlet flow rate is 382,331 lb/hr, inlet quality is 92.15% and outlet pressure is 420 psia. Fig. 4 demonstrates the droplet characteristics within the FWH shell side in the three dimensional plot (a) and the two dimensional plot (b) from the front view, respectively. The color index in the upper left corner indicates the magnitude of the droplet velocity. This figure clearly reveals that droplets enter from the inlet, bounce off the impingement plate, impinge on the shell wall and finally flow along the shell wall to the bottom of the FWH. In addition, the incoming droplets lose velocity as they collide with the impingement plate, which can be shown in the color change (from red to blue) for the droplet velocity.[1]

Fig. 4b indicates that most of the droplet-wall collisions will occur at the locations around the edge of the impingement plate and the altitude of the collision locations is a little higher than that of the impingement plate. These results are also shown in Fig. 5 that displays the positions of droplet-wall collisions (white dots in this figure) from the top view. These droplets colliding with the shell wall will cause wall thinning through the droplet impingement wear mechanism. The width of these collisions is slightly larger than that of the impingement plate and less than four times the inlet tube diameter, which is similar to the measuring range suggested by the Electric Power Research Institute (EPRI) [38]. These predicted results can be confirmed in Fig. 6 that shows the photographs of wear sites on the high pressure FWH shell wall. The photographs are taken from the inside of the shell and are cut from the center of the inlet tube to present clearly the wear sites of both sides. In addition, Fig. 6 clearly reveals that the range of wear sites for the right side is larger than that for the left side, which is precisely captured by the present models and is discussed in the following.

Using the ultrasonic transmitter (UT), the power plant staff can measure the thickness of the FWH shell wall during the plant outage. These raw data of wall thickness are smoothed by the so called "ring smoothing method" as suggested by the Electric Power Research Institute

[1] For interpretation of color in Figs. 4 and 5, the reader is referred to the web version of this article.

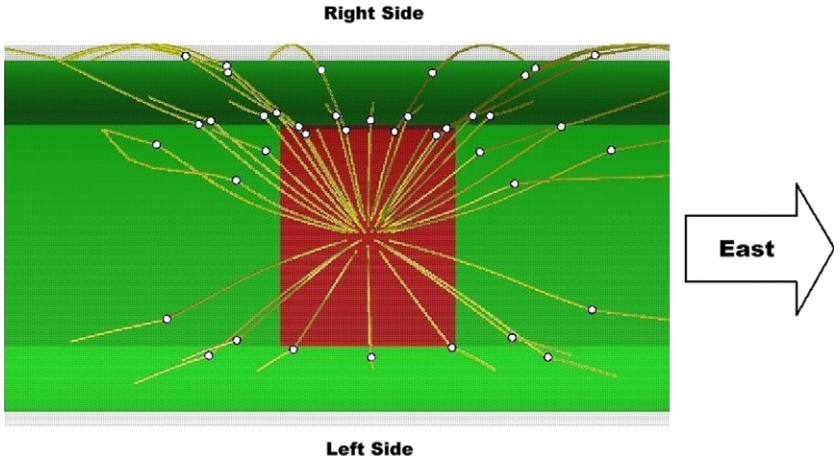

Fig. 5. Distribution characteristics of droplet-wall collisions on a high pressure FWH shell wall.

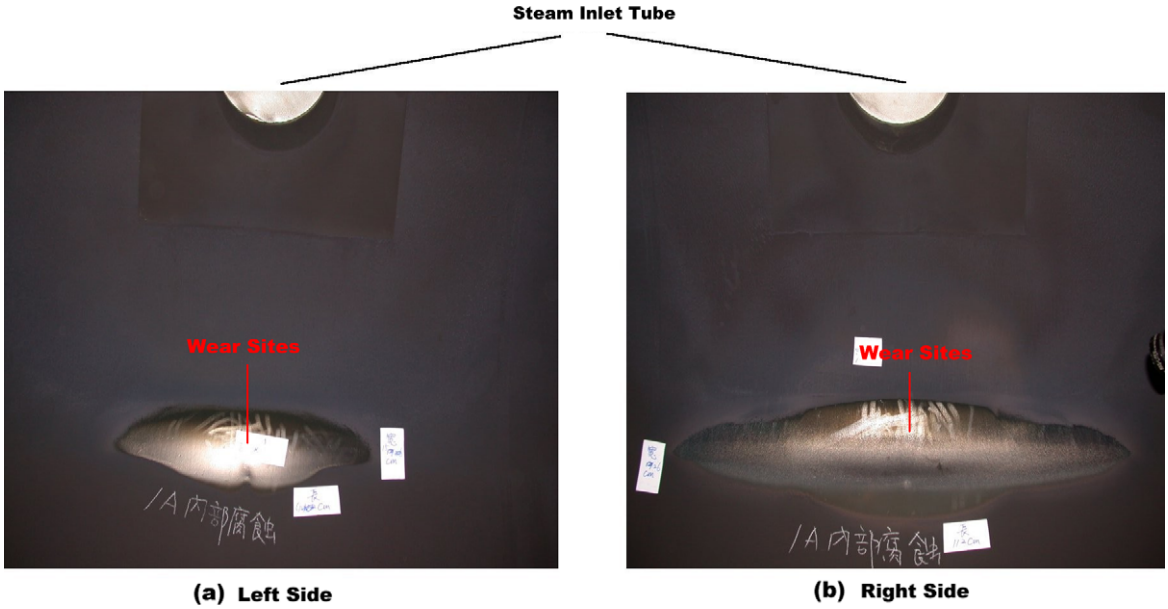

Fig. 6. Comparison of severe wear sites on a high pressure FWH shell wall between measured data and predicted results.

(EPRI) [38]. The plant measured data of wear sites can be derived by differencing two measurements of wall thickness. Based on the wear site expression suggested by the CHEC program [38], the degree of black qualitatively represents the wear thickness and indicates the severity of the wear sites. In other words, the blackest region is the location where the wall thinning is the most severe, and the white region is the location where no wear phenomenon occurs. This presentation is demonstrated in Fig. 7 that shows the plant measured wear sites (a) and the calculated results (b). The plots in this figure are two dimensional plots for the wear sites on the FWH shell wall, which are unfolded from the centerline of the opposite side of the steam inlet tube. Similar to previous works [17–19], an appropriate indicator derived from Eq. (2.21) is used to indicate the locations of severe wear sites on the FWH shell wall, which is shown in Fig. 7b. In this figure, the blacker the color is, the more severe the impingement wear is. The wear sites predicted by the present model correspond well with the plant measured data, as is clearly demonstrated in Fig. 7. In order to display clearly the range of wear sites, these measured and predicted results are put on the FWH shell wall, which is shown in (left side) Figs. 8 and 9 (right side), respectively. These two figures also reveal the good agreement between the measured (represented by red) and the predicted wear ranges (represented by green). As discussed in the previous subsection, Figs. 7–9 for both the measurement and prediction confirm the impingement wear for the right side of the shell wall is more severe than that for the left side.

The simulation results presented about are concentrated in the high pressure FWH. A low pressure FWH is selected to assess the two phase models proposed in this paper. The

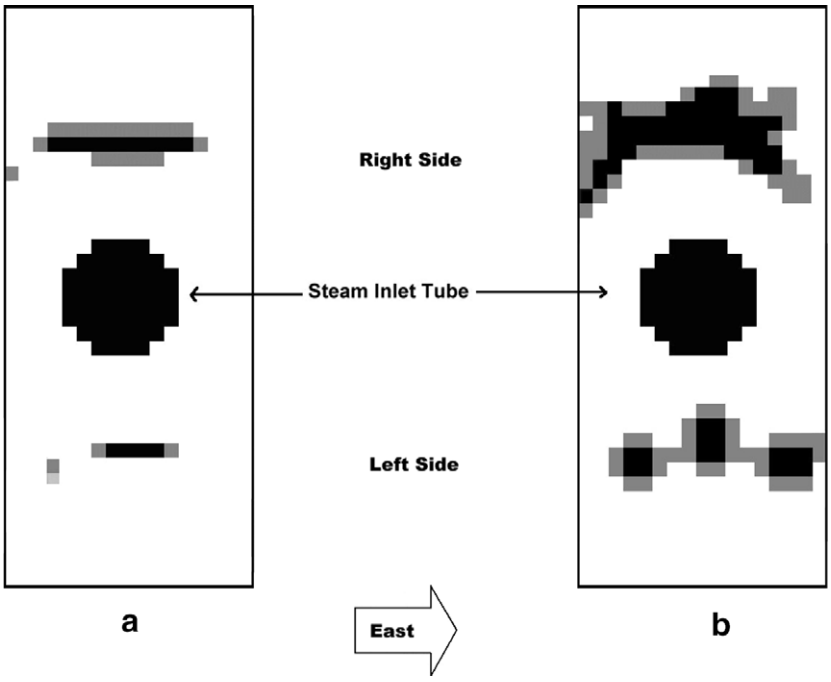

Fig. 7. Photographs of wear sites on a high pressure FWH shell wall.

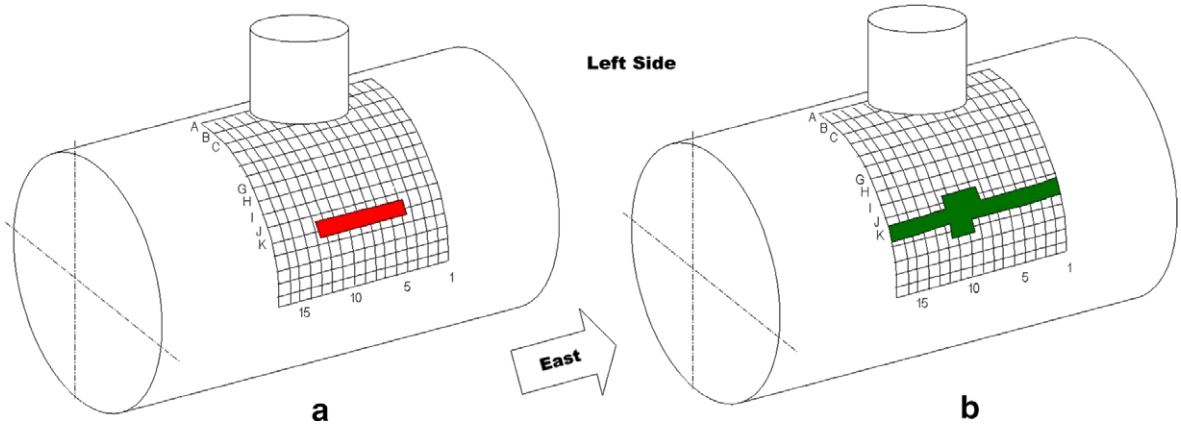

Fig. 8. Schematic of wear sites on the left side of shell wall (red: measurement, green: prediction) (For interpretation of the references in colour in this figure legend, the reader is referred to the web version of this article.).

flow conditions of inlet steam for this heater are: inlet temperature is 338 °F; inlet flow rate is 211,913 lb/h; inlet quality is 98.1%; and outlet pressure is 118.9 psia. This low pressure FWH is connected to the condenser through an elbow. Therefore, this upstream elbow must be modeled in the simulation. Fig. 10 shows the droplet characteristics around the inlet tube, impingement plate and shell wall. Plot (a) shows the droplet tracks in the three dimensional form, and plot (b) shows them in a two dimensional form based on the front view. The droplets carried by the steam enter downward into the shell, collide with the impingement plate and subsequently rebound dispersedly to the downstream side. Because of the geometry of the inlet elbow, the heavier liquid droplets will be pushed to the extremes of the elbow, rendering more droplets bouncing west (x direction) after they collide with the impingement plate. This phenomenon results in most of the droplet-wall collisions being located near the downstream side of the impingement plate edge, as is clearly shown in Fig. 11. This figure demonstrates the locations (white dots) of the droplet-wall collisions on the shell wall of a low pressure FWH from the top view. Similar to the presentation in Figs. 7 and 12 shows the comparison of droplet impingement wear sites for the plant measured data (a) and the calculated results (b). In these plots, the blacker regions represent the more severe wear sites. It must be noted that the unfolded region shown in this figure contains a steam tube and a vent tube. These tubes are presented as the black

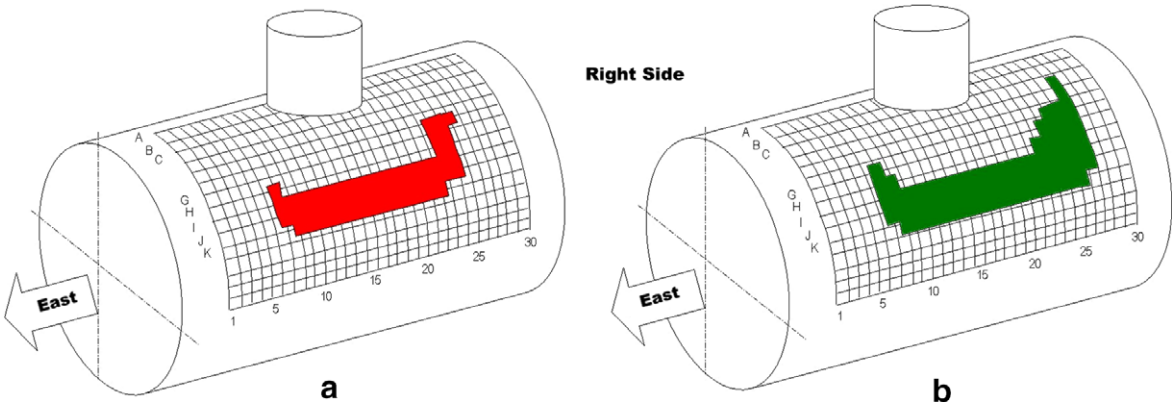

Fig. 9. Schematic of wear sites on the right side of shell wall (red: measurement, green: prediction) (For interpretation of the references in colour in this figure legend, the reader is referred to the web version of this article.).

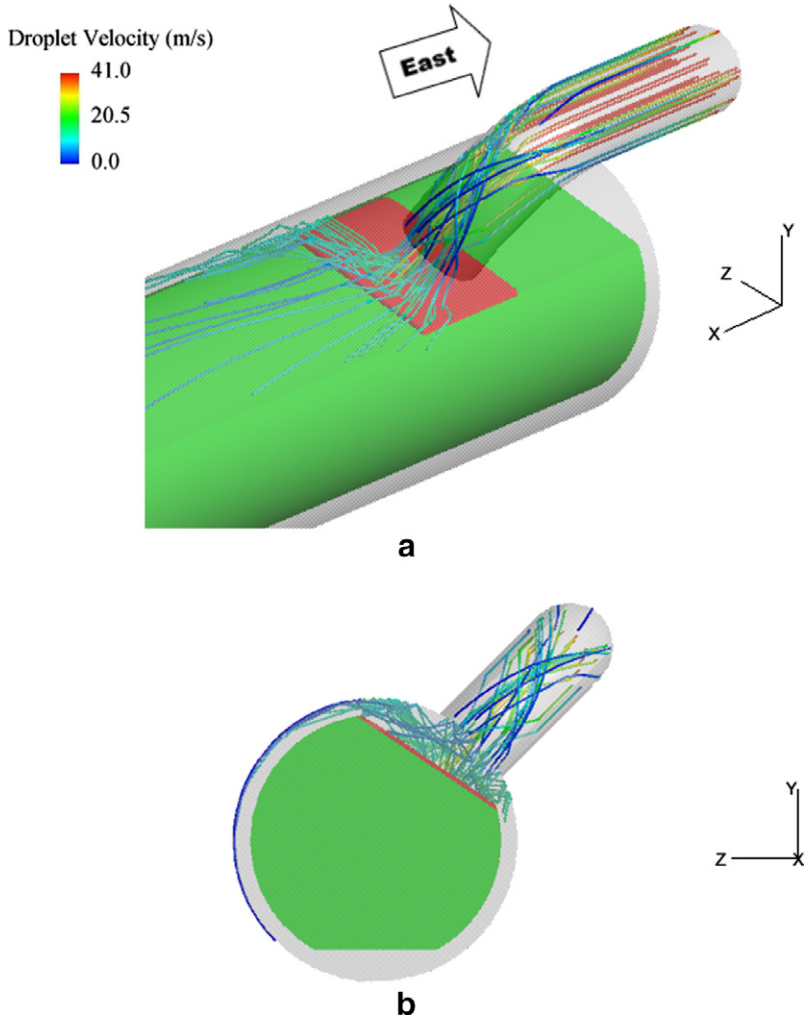

Fig. 10. Flow characteristics of liquid droplets within a low pressure FWH shell.

regions that are denoted as "Steam Inlet Tube" and "Vent Tube", respectively. The comparison from Fig. 12 clearly reveals that the impingement wear sites predicted by the present two phase models (plot (b)) show good agreement with the measured data (plot (a)). As in the aforementioned discussion, most of droplet-wall collisions are located near the downstream side of the impingement plate edge. Severe wall thinning locations would then be shifted there (i.e. to

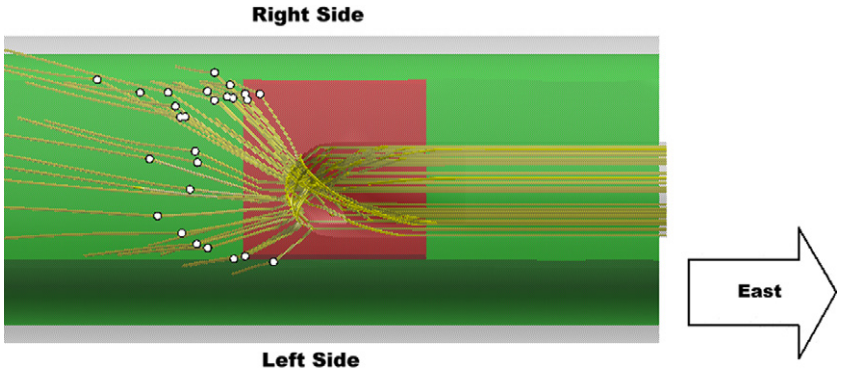

Fig. 11. Distribution characteristics of droplet-wall collisions on a low pressure FWH shell wall.

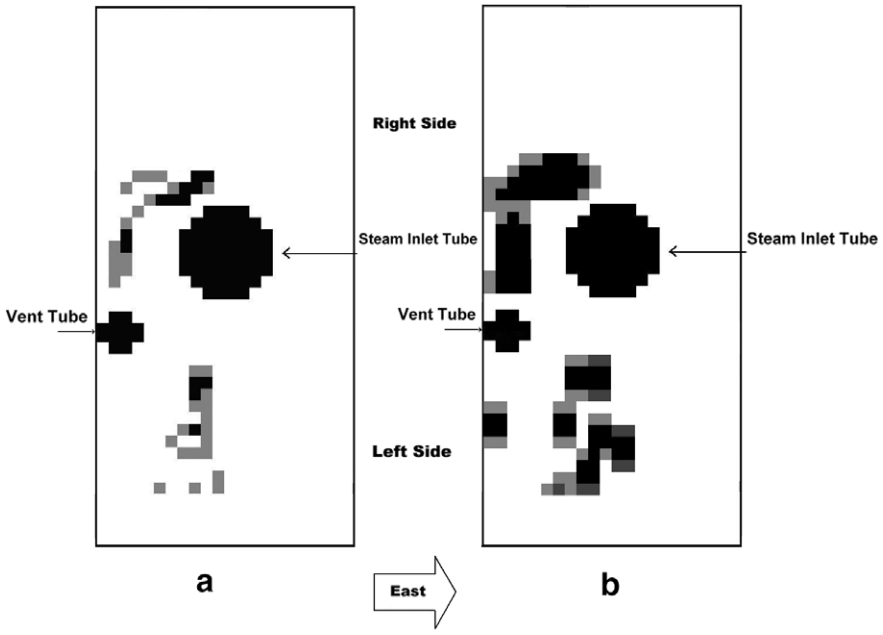

Fig. 12. Comparison of severe wear sites on a low pressure FWH shell wall between measured data and predicted results.

the west). Both the measured and calculated results confirm this conclusion.

5. Conclusions

Two phase models, which include the Eulerian/Lagrangian two phase flow model and the droplet impingement wear model, are proposed in this paper to investigate the characteristics of droplet flow and predict the distributions of impingement wear sites for the FWH. Both the high pressure and low pressure FWHs in the PWR are selected to assess these models. Several important conclusions are drawn from the simulation results.

1. The Eulerian/Lagrangian two phase flow models can reasonably capture the characteristics of the droplet flow within the FWH's shell side, which include the three dimensional distribution of droplet flow, droplet impingement and droplet rebound behaviors on the solid wall.
2. Based on the predicted results of droplet-wall collisions, the wear sites are distributed on the shell wall near the impingement plate, and their ranges are less than four times the width of the tube diameter, which are similar to the EPRI suggestion [38].
3. Compared with the plant measured data, the wear sites predicted by the present two phase models show good agreement. The unsymmetrical distribution patterns of wear sites are also precisely captured. These correspondences are demonstrated for both the high pressure and low pressure FWHs, which reveals that the present two phase models can be used to investigate the flow characteristics, droplet impingement and impingement wear within the FWHs of the nuclear power plant.

References

[1] Crowe CT, Sharma MD, Stock DE. The particle-source-in-cell model for gas-droplet flows. J Fluid Eng 1997;99:325–32.

[2] Dukowicz JK. A particle-fluid numerical model for liquid sprays. J Comput Phys 1980;35:229–53.
[3] Theofanous T, Sullivan J. Turbulence in two-phase dispersed flows. J Fluid Mech 1982;116:343–62.
[4] Berlemont A, Desjonqueres P, Giusbet G. Particle Lagrangian simulation in turbulent flows. Int J Multiphase Flow 1990;16:19–34.
[5] Yuan X, Michaelides EE. Turbulent modulation in particulate flows-a theoretical approach. Int J Multiphase Flow 1992;18:779–85.
[6] Webb C, Que F, Senior PR. Dynamic simulation of gas–liquid dispersion behaviour in a 2-D bubble column using a graphics mini-super-computer. Chem Eng Sci 1992;47:3305–12.
[7] Elghobashi S. On predicting particle-ladden turbulent flows. Appl Sci Res 1994;52:309–24.
[8] Lapin A, Lubbert A. Numerical simulation of the dynamics of two-phase gas–liquid flow in bubble columns. Chem Eng Sci 1994;49: 3661–74.
[9] Chen XQ, Pereira JCF. Computation of turbulent evaporating sprays with well-specified measurements: a sensitivity study on droplet properties. Int J Heat Mass Transfer 1994;34:441–54.
[10] Graham DI. An improved eddy interaction model for numerical simulation of turbulent particle dispersion. J Fluid Eng 1996;118: 819–23.
[11] Graham DI, James PW. Turbulent dispersion of particles using eddy interaction models. Int J Multiphase Flow 1996;22(1):157–75.
[12] Pokharna H, Mori M, Ransom VH. The particle fluid model and using Lagrangian representation in two-phase flow modeling. Nucl Eng Des 1997;175:59–69.
[13] Chen XQ, Pereira JCF. Computation of particle-laden turbulent gas flows using two dispersion models. AIAA J 1998;36:539–46.
[14] Chen XQ. Heavy particle dispersion in inhomogeneous, anisotropic, turbulent flow. Int J Multiphase Flow 2000;26:635–61.
[15] Poirer DR. Permeability for flow of interdendritic liquid in columnar-dendritic alloys. Metall Trans 1987;18B:245.
[16] Lee SL, Yang JH. Modeling of Darcy-Forchheimer drag for fluid flow across a bank of circular cylinders. Int J Heat Mass Transfer 1997;40(13):3149.
[17] Ferng YM et al. A physical model to predict wear sites engendered by flow-assisted corrosion. Nucl Technol 1999;126(3):319–30.
[18] Ferng YM et al. A new approach to investigate erosion/corrosion phenomenon through the local flow models. Corrosion 1999;44(4): 332–42.
[19] Ferng YM et al. Application of local flow models in predicting the distributions of erosion–corrosion locations. Corrosion 2000;56(2): 116–26.
[20] Catapano M, Krzywosz K, Tsou J. Feedwater heater technology seminar. In: Feedwater heater technology seminar and symposium, EPRI, Palo Alto, CA, October 1998.
[21] Ergun S. Fluid flow through packed columns. Chem Eng Progr 1952;48:89.
[22] Blake FC. The resistance of packing to fluid flow. AIChE J 1922;14:415.
[23] Cheng P, Hsu CT. Applications of Van Driest's mixing length theory to transverse, thermal dispersion in a packed-bed with boundary walls. Int Commun Heat Mass Transfer 1986;13:613.
[24] Launder BE, Spalding DB. The numerical computational of turbulent flows. Comput Methods Appl Mech Eng 1973;3:269.
[25] CFX-4.2: User Manual, Computational Fluid Dynamics Services, 1997.
[26] Wallis GB. One-dimensional two-phase flow. New York: McGraw-Hill; 1969.
[27] Remy FN, Bouchacourt M. Flow-assisted corrosion: A method to avoid damage. Nucl Eng Des 1992;133:23.
[28] Sha WT, Launder BE. A general model for turbulent, momentum and heat transfer in liquid metals. ANL-77-78, Argonne National Laboratory, 1979.
[29] Adams GG. Imperfectly constrained planar impacts-a coefficient-of-restitution model. Int J Impact Eng 1997;19(8):693–701.
[30] Thornton C, Ning Z. A theoretical model for the stick/bounce behaviour of adhesive elastic–plastic spheres. Powder Technol 1998;99:154–62.
[31] Brach RM, Dunn PF. Models of rebound and capture for oblique microparticle impacts. Aerosol Sci Technol 1998;29:379–88.
[32] Kleis I, Hussainova I. Investigation of particle-wall impact process. Wear 1999;233:168–73.
[33] Sommerfeld M, Huber N. Experimental analysis and modelling of particle-wall collisions. Int J Multiphase Flow 1999;25:1457–89.
[34] Gorham DA, Kharaz AH. The measurement of particle rebound characteristics. Powder Technol 2000;112:193–202.
[35] Patankar SV. Numerical heat transfer and fluid flow. New York: Hemisphere Publishing Company; 1981.
[36] Patankar SV, Spalding DB. A calculation procedure for heat, mass and momentum transfer in parabolic flows. Int J Heat Mass Transfer 1972;15:1787.
[37] Spalding DB. Modelling a body-fitted-coordinate grid during a PHOENICS computation. CHAM/PER/88/1, Wimbledon Village, London, United Kingdom.
[38] Chexal VK, Horowitz JS. CHEC computer program user's manual. Nuclear Safety Analysis Center (NSAC) 112L, R2, Electric Power Research Institute, 1989.